

# Indium–Organic Framework with *soc* Topology as a Versatile Catalyst for Highly Efficient One-Pot Strecker Synthesis of $\alpha$ -aminonitriles

Gaurav Verma, Katherine Forrest, Benjamin A. Carr, Harsh Vardhan, Junyu Ren, Tony Pham, Brian Space, Sanjay Kumar,\* and Shengqian Ma\*

Cite This: *ACS Appl. Mater. Interfaces* 2021, 13, 52023–52033

Read Online

ACCESS |

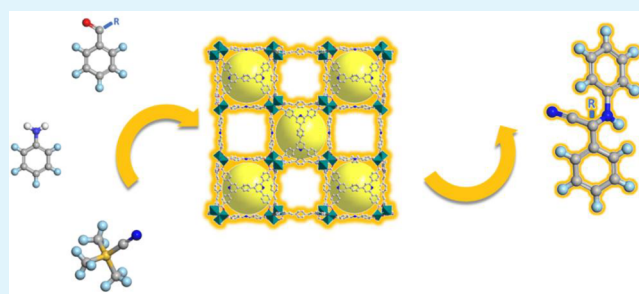
Metrics & More

Article Recommendations

Supporting Information

**ABSTRACT:** An In(III) based metal–organic framework (MOF), In-pbpta, with *soc* topology was constructed from the trigonal prismatic  $[\text{In}_3(\mu_3\text{-O})(\text{H}_2\text{O})_3(\text{O}_2\text{C-})_6]$  secondary building unit (SBU) and a custom-designed tetratopic linker  $\text{H}_4\text{pbpta}$  (pbpta = 4,4',4'',4'''-(1,4-phenylenbis(pyridine-4,2,6-triyl))-tetrabenzoic acid)). The obtained MOF shows a Brunauer–Emmett–Teller surface area of 1341  $\text{m}^2/\text{g}$  with a pore volume of 0.64  $\text{cm}^3/\text{g}$ , which is the highest among the scarcely reported In-*soc*-MOFs. The constructed MOF demonstrates excellent performance as a heterogeneous Lewis acid catalyst for highly efficient conversion in a one-pot multicomponent Strecker reaction for the preparation of  $\alpha$ -aminonitriles under solvent-free conditions, which can be easy to separate and recycle without significant loss of activity for up to seven cycles. The computational modeling studies suggest the presence of the three substrates in close vicinity to the In-oxo cluster. The strong interactions of the aldehyde/ketone and the amine with the In-oxo cluster together with the readily available cyanide ion around the In-oxo cluster lead to high catalytic conversion within a short period of time for the MOF catalyst. Our work therefore lays a foundation to develop MOF as a new class of efficient heterogeneous catalyst for one-pot Strecker reaction.

**KEYWORDS:** indium–organic framework, Strecker reaction, one-pot, recyclability, computational modeling



## 1. INTRODUCTION

Over the past century, economic and social progress has been accompanied by harmful impacts on the environment such as climate change, declining soil fertility, and degradation of the aquatic environment.<sup>1,2</sup> For a sustainable future, the production patterns need to be transitioned toward a greener approach that can promote environmentally sound management of chemicals and waste production and markedly reduce their release into air, water, and soil.<sup>3</sup> One-pot processes can play an important role in this regard, reducing the reliance on polluting and traditional mindsets of chemical production.<sup>4–6</sup>

Strecker reaction is among the oldest and most crucial one-pot multicomponent reactions involving the condensation of an aldehyde/ketone with an amine in the presence of a cyanide source to generate  $\alpha$ -aminonitriles.<sup>7</sup> These  $\alpha$ -aminonitriles are precursors to amino acids, the backbone of all living systems on earth. Traditionally homogeneous Lewis acid catalyst,<sup>8</sup> organocatalysts,<sup>9</sup> and ionic liquids<sup>10</sup> have been used to catalyze the reaction, but usually these are accompanied by tedious purification and high waste generation.<sup>7,11,12</sup> Heterogeneous catalysts, on the other hand, offer several advantages such as recyclability and reduced waste formation. However, they

suffer from key challenges as in loss of activity and lower efficiencies.<sup>7,8</sup>

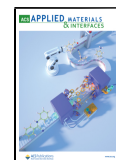
Over recent years, metal–organic frameworks (MOFs) have come at the forefront of heterogeneous catalysis because of their ordered structures, tailorability for the desired application, and high efficiencies compared to the traditional systems.<sup>13–15</sup> MOFs are porous materials constructed from metal clusters or secondary building units (SBUs) connected by organic linkers and endowed with high crystallinity, structural diversity, high porosity, ease of functionalization, and presence of a high density of active sites.<sup>16,17</sup> MOFs as heterogeneous catalysts have shown remarkable efficiencies in some of the relevant catalytic processes for organic transformations.<sup>18–20</sup> The features that set MOFs apart are the high-precision designability, ideal and tunable pore characteristics for incorporating catalytic species, potential to affix

**Special Issue:** Emerging Materials for Catalysis and Energy Applications

**Received:** May 16, 2021

**Accepted:** June 18, 2021

**Published:** July 1, 2021



catalytic sites on both the inorganic and organic components, and confined spaces for the specific reaction environment.<sup>14,21–23</sup>

In this context, group 13 elements such as indium based materials have been emerging as fundamentally reliable catalysts due to their versatile coordination numbers, ability to provide facile Lewis acidic sites, good thermal stability, and accessible high-level p-orbitals of the In<sup>3+</sup> cation and its unique electronic configuration that gives it a varying binding affinities to a myriad of coordinated atoms enabling the structure-directed synthesis.<sup>24–26</sup> Furthermore, indium is much less toxic compared to the other catalysts, making it green and environmentally benign. The indium-oxo clusters in particular have shown a plethora of possibilities to catalyze various organic transformations including CO<sub>2</sub> hydrogenation to methanol, transformation of epoxides and CO<sub>2</sub> into valuable cyclic carbonates, and various multicomponent reactions.<sup>26–31</sup> The utilization of indium organic frameworks (InOFs) in the Strecker reaction was first explored by Xia et al.,<sup>27</sup> for the reaction of aldimines with TMSCN. Aguirre-Diaz et al.<sup>28</sup> demonstrated the capability of the InOFs to directly catalyze the one-pot Strecker reaction between benzaldehyde, aniline, and TMSCN; however, the catalytic activity with ketones was less compared to the aldehydes. Advancing the research further to expand InOFs for widespread applicability using ketones, in 2016 Reinares-Fisac, Monge and Gandara et al.<sup>29</sup> developed the InP-F110 that displayed outstanding catalytic activity for the Strecker reaction of ketones to give the substituted  $\alpha$ -aminonitriles. Since then, several indium and non-indium based catalysts were developed for this reaction. However, only a few SBUs such as monomeric [In(CO<sub>2</sub>)<sub>n</sub>]<sub>n</sub>, trimeric [In<sub>3</sub>O(CO<sub>2</sub>)<sub>n</sub>(OH<sub>2</sub>)<sub>n</sub>], and chain-like [In(O or OH)]<sub>n</sub> have been employed and new InOFs with novel structures and fine-designed functionalization are highly desirable.<sup>26,32–34</sup>

Bearing those above in mind, we set out to utilize trigonal prismatic metal SBUs [In<sub>3</sub>( $\mu_3$ -O)(-COO)<sub>6</sub>] and rectangular/square tetratopic organic linker (H<sub>4</sub>pbpta) to construct the MOF In-pbpta with *soc* topology, isostructural to the MOF Fe-pbpta reported by us recently.<sup>35</sup> The *soc*-MOFs display highly microporous architectures having well-defined cages and channels consisting of narrow pores with higher localized charge density.<sup>36–38</sup> The advantage of these materials is that they exhibit superior properties such as a high degree of porosity, high storage capacities, and good thermal stability. Numerous examples of robust *soc*-MOFs<sup>36,39–49</sup> have been established utilizing the reticular chemistry approach.<sup>50</sup> However, these *soc*-MOFs have rarely been explored in catalysis. In this work, the robust MOF In-pbpta with dense active indium sites displayed very high catalytic efficiency in one-pot multicomponent synthesis of  $\alpha$ -aminonitriles under solvent-free conditions at room temperature. Moreover, the catalyst can be recycled up to seven cycles with good catalytic activities followed by a start of some loss in activity and crystallinity after the eighth cycle. Theoretical investigations were also carried out to elucidate the interactions involved and the subsistence for the observed high catalytic activity.

## 2. EXPERIMENTAL SECTION

**2.1. General Methods.** All reagents and solvents were purchased from commercial sources and used as received. The ligand H<sub>4</sub>pbpta was synthesized using our previously reported procedure.<sup>51</sup>

**2.1.1. MOF Synthesis.** A mixture of the ligand H<sub>4</sub>pbpta (10 mg, 0.01 mmol) and In(NO<sub>3</sub>)<sub>3</sub>·3H<sub>2</sub>O (20 mg, 0.05 mmol) was dissolved

in a 20 mL scintillation vial containing DMF (1 mL), CH<sub>3</sub>CN (0.5 mL), HNO<sub>3</sub> (10  $\mu$ L, 2.7 M), and piperazine (50  $\mu$ L, 0.4 M). The reagents were sonicated to dissolve them completely and placed in an oven at 85 °C for 24 h to yield yellow cubic crystals. Yield: 74.2% (based on the ligand), FT-IR (cm<sup>-1</sup>):  $\nu$  = 3061 (w, br.), 1593 (s), 1545 (m), 1383 (s), 1178 (w), 1104 (w), 1015 (m), 863 (w), 817 (m), 784 (s).

**2.1.2. Characterization.** Powder X-ray diffraction (PXRD) data were collected at room temperature using a Bruker D8 Advance  $\theta$ - $2\theta$  diffractometer with copper radiation (Cu  $K\alpha$  = 1.5406 Å) and a secondary monochromator operating at 40 kV and 40 mA, whereby samples were measured between 2° and 40° at 0.5 s/step and step size of 0.01°. Infrared spectra measurements from 4000 to 400 cm<sup>-1</sup> were taken on a PerkinElmer FT-IR spectrometer Spectrum Two (UATR Two) with 4 cm<sup>-1</sup> resolution. A TA Instruments TGA Q50 was used to record thermal gravimetric analysis (TGA) data from room temperature to 600 °C at a 10 °C/min rate. A Varian Unity Inova 400 spectrometer NMR was used to measure <sup>1</sup>H NMR. GC-MS measurements were performed on an Agilent GC-MSD 5977B using a ZB-5 column. Gas adsorption measurements were performed using a Micromeritics ASAP 2020 analyzer for N<sub>2</sub> (surface area measurement at 77 K) and CO<sub>2</sub> and CH<sub>4</sub> isotherms at 273 and 298 K.

**2.2. Catalytic One-Pot Strecker Reaction.** The catalyst In-pbpta was first activated by soaking in acetonitrile for 5 days, and the acetonitrile was changed three times per day. Then it was heated at 100 °C under dynamic vacuum for 6 h in a Schlenk tube. For a typical Strecker reaction, a mixture of aldehyde/ketone (0.85 mmol), amine (0.77 mmol), and trimethylsilyl cyanide (0.85 mmol) was added to the Schlenk tube having the catalyst (10 mg, 0.88 mol %), and stirred at room temperature for 30 min in solvent-free condition under an N<sub>2</sub> atmosphere. The progress and completion of the reaction was monitored by GC-MS and <sup>1</sup>H NMR. The yield was calculated from the <sup>1</sup>H NMR and/or GC-MS data. After the completion of the reaction, the mixture was diluted with chloroform and the catalyst was separated by centrifugation followed by washing with acetonitrile (5 mL, three times). The recovered catalyst was dried at 100 °C before reuse in the next cycle.

**2.3. Computation and Modeling.** Computational modeling of MOF/reagent interactions initially required parametrization for classical simulation using the massively parallel Monte Carlo code.<sup>52</sup> In-pbpta was treated using the OPLS<sup>53,54</sup> and UFF<sup>55</sup> van der Waals force fields, EQ charge fitting<sup>56</sup> to model electrostatics, and induced dipole effects approximated using Thole–Applequist type point polarizabilities as used in previous indium *soc*-MOF simulation studies.<sup>57</sup> The reagents, as well as the nitrate counterions which were not resolved in the X-ray crystal structure, were relaxed and charge-fit using the NWChem simulation package.<sup>57,58</sup> The sorbate van der Waals and induction energetic were modeled in the same manner as the crystal structure.

A series of classical simulated annealing simulations were then run on the mobile reagents and counterions in the rigid single unit cell crystal framework in order to provide rough initial positions about the indium clusters. Once the minima were obtained, a fragment of the MOF containing the indium cluster, attendant sorbates, and a proximal counterion was subjected to density functional theory (DFT) geometry optimization. This relaxation of the reagents and counterion took place about the rigid crystal fragment and employed MOLOPT exchange and triple  $\zeta$  basis sets using the CP2K code.<sup>58–78</sup>

## 3. RESULTS AND DISCUSSION

**3.1. Structural Characterization.** The solvothermal reaction of H<sub>4</sub>pbpta with In(NO<sub>3</sub>)<sub>3</sub>·3H<sub>2</sub>O in a solution of DMF/CH<sub>3</sub>CN with HNO<sub>3</sub> and piperazine as the modulators afforded In-pbpta as yellow cubic crystals (size  $\sim$  20  $\mu$ m; Supporting Information (S1) Figure S1) characterized by single crystal X-ray diffraction (SCXRD) as [In<sub>3</sub>O(pbpta)<sub>1.5</sub>(H<sub>2</sub>O)<sub>3</sub>](NO<sub>3</sub>). It crystallizes in the cubic *Pm* $\bar{3}$ *n* space group with a periodic framework built from  $\mu_3$ -oxo-centered trinuclear

In(III) SBUs  $[\text{In}_3(\mu_3\text{-O})(\text{H}_2\text{O})_3(\text{O}_2\text{C-})_6]$  and the rectangular linker pbpta<sup>4-</sup> (Figure 1).

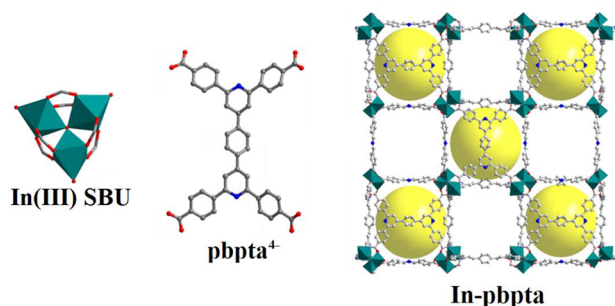


**Figure 1.** Crystal structure of In-pbpta showing the assembly of the trinuclear indium(III) MBB  $[\text{In}_3(\mu_3\text{-O})(\text{H}_2\text{O})_3(\text{O}_2\text{C-})_6]$  with the organic ligand pbpta<sup>4-</sup>.

Each of the  $\text{In}^{3+}$  cations shows an octahedral coordination environment and coordinates to six oxygen atoms, four from bis-monodentate deprotonated carboxylate oxygen atoms from four independent pbpta<sup>4-</sup> ligands and one  $\mu_3$ -oxo anion, and a terminal water molecule to complete the coordination sphere. The In(III) SBUs were bridged by six independent pbpta<sup>4-</sup> ligands to give the three-periodic cationic framework with *soc*-topology (Figure 1), isostructural to the MOF Fe-pbpta reported recently by our group.<sup>35</sup> The anions in the structure are disordered and difficult to locate because of the high symmetry, which were modeled as nitrate<sup>35</sup> to provide the countercharge. The framework has similar cubic cages with dimensions of 16.2 Å, and the solvent accessible free volume for In-pbpta was estimated to be 82.4% using the PLATON software.<sup>79</sup>

The phase purity of the bulk sample was confirmed by comparing the calculated PXRD pattern to that of the bulk phase sample, which was in good agreement with each other (Figure S2).<sup>86</sup> Also, the material further showed a high thermal stability up to around 400 °C from the TGA analysis after an initial solvent loss (Figure S3).

**3.2. Gas Adsorption Studies.** Owing to the microporous architecture of the In-pbpta and the well-defined cages and

channels as evidenced from the structure, it was subjected to gas adsorption measurements to investigate the pore characteristics. The as-synthesized sample was first activated by solvent exchange with acetonitrile (5 days, 3 × 5 mL), followed by the guest solvent removal using the conventional conditions of vacuum and heating without altering the microporosity.

The nitrogen ( $\text{N}_2$ ) adsorption–desorption measurements carried out at 77 K on the acetonitrile exchanged samples showed a fully reversible type-I isotherm characteristic of the microporous materials (Figure 2a). The maximum uptake observed was 414  $\text{cm}^3/\text{g}$  corresponding to BET and Langmuir surface areas of 1341 and 1541  $\text{m}^2/\text{g}$ , respectively, with a pore volume of 0.64  $\text{cm}^3/\text{g}$ . The pore size distribution was calculated using the density functional theory model and found pores of width less than 18 Å (Figure 2b). It is worth noting that In-pbpta has the highest surface area among all the indium *soc*-MOFs reported so far (Table S1).<sup>36,42,43,45,47,80</sup> It can be assumed that the extended linker leads to an increase in the pore width and hence an overall increase in surface area compared to the other In-*soc*-MOFs.

Low-pressure gas adsorption isotherms were also obtained using  $\text{CO}_2$  and  $\text{CH}_4$ . The In-pbpta showed maximum  $\text{CO}_2$  uptake capacities of 50 and 27  $\text{cm}^3/\text{g}$  at 273 and 298 K, respectively (Figure S4a), with a relatively high- $Q_{\text{st}}$  value of 25.7 kJ/mol (Figure S5) indicating the presence of fine-tuned pores and strongly interacting accessible unsaturated metal centers with a high affinity for the adsorbate. In the case of  $\text{CH}_4$ , much lower uptake capacities of 12 and 8  $\text{cm}^3/\text{g}$  were obtained at 273 and 298 K, respectively, due to the nonpolar nature of the methane molecules (Figure S4b).

After establishing the high porosity, good thermal stability, and moderately strong adsorbate–MOF interactions for In-pbpta, we subsequently turned our attention to investigating its catalytic application.

**3.3. Catalytic Activity for Strecker Reaction.** The  $\alpha$ -aminonitriles are used as important building blocks in pharmaceutical industry, heterocyclic chemistry, and agrochemicals, among others.<sup>7</sup> A great molecular diversity with a high degree of complexity can be achieved for these compounds. Since it requires a great deal of complexity to assemble these multiple reactants to selectively produce the

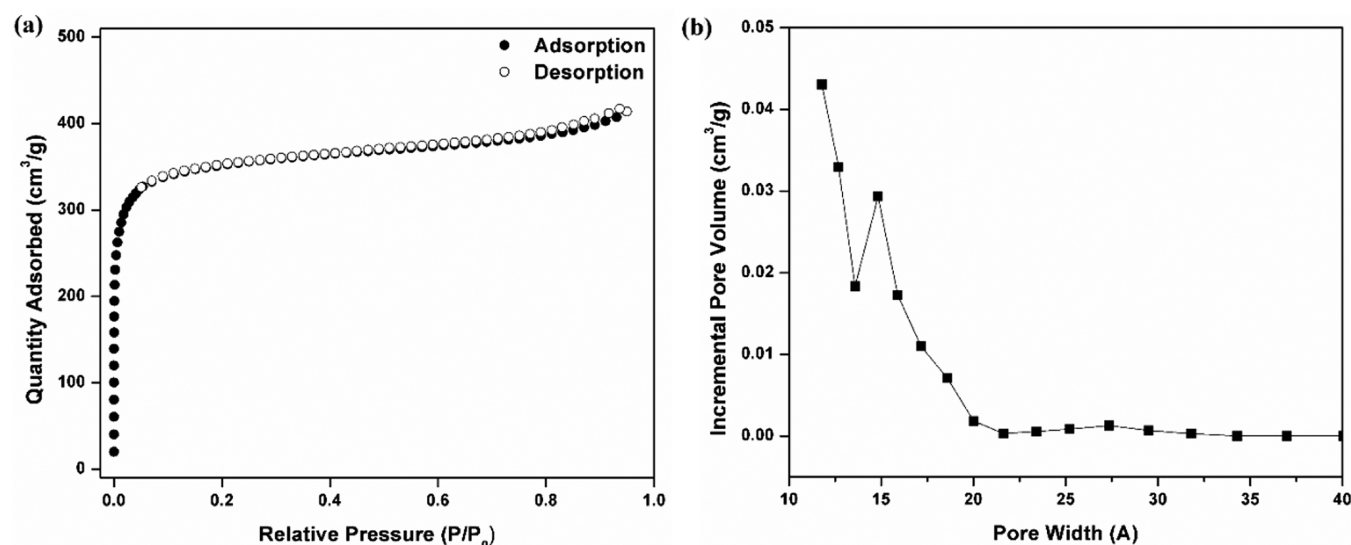
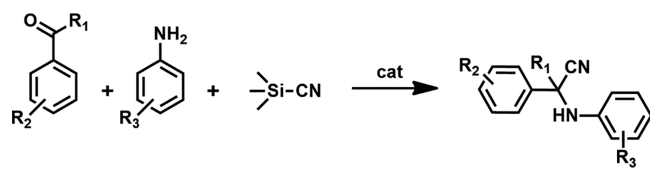


**Figure 2.** (a) Nitrogen adsorption–desorption at 77 K for In-pbpta showing fully reversible type-I isotherm and (b) pore size distribution.

desired  $\alpha$ -aminonitrile product, often complex catalytic systems need to be used. The Strecker reaction is generally catalyzed by Lewis acid catalysts that lead to the facile activation of the carbonyl group which is in turn combined with amine to generate iminium intermediate. The iminium intermediate is further attacked by a  $\text{CN}^-$  from a cyanide source such as TMS-CN to give the corresponding  $\alpha$ -aminonitrile.<sup>7</sup> A general schematic of the Strecker reactions is depicted in Scheme 1.

**Scheme 1. Strecker Reaction between an Aldehyde/Ketone, Amine, and TMS-CN to Give the Desired  $\alpha$ -Aminonitrile Product**



To establish the ability of In-pbpta to catalyze the Strecker reaction, we first started with aldehyde as the carbonyl substrate and reacted benzaldehyde, aniline, and TMS-CN. The MOF catalyst was activated at 100 °C under vacuum prior to carrying out the test in a Schlenk tube at room temperature under a nitrogen atmosphere in solvent-free conditions. The final product was selectively obtained with a yield of 99% (Table 1, entry 1) in 30 min at a catalyst loading of 0.88 mol %

(the optimization of the catalyst loading is provided in Table S2 of the SI).

Now, a plethora of reports using a variety of catalysts are documented in the literature for the generation of  $\alpha$ -aminonitriles from aldehydes, whereas with ketones it remained challenging.<sup>7</sup> Often, the catalysts used in this reaction with ketone precursors are accompanied by some drawbacks such as low conversion, separation of products, low efficacy, or prolonged time durations.<sup>7,9</sup> In 2016, Monge et al. demonstrated exceptional catalytic activity for the Strecker reaction of ketones with various amines having high turnover numbers (TONs) using InPF-110, opening up the avenue for the utilization of MOFs as the catalysts for Strecker reactions of ketone substrates.<sup>29</sup> However, better and more efficient catalytic systems are still needed for widespread applicability and an understanding of the host-substrate system is necessary for improved design and performance.

Therefore, we extended our protocol for the reaction of ketones with aniline as the amine (Table 1). To our delight, when acetophenone was used, excellent result (98% yield) was obtained (Table 1, entry 2) within the same time duration of 30 min. We have summarized the activity of the prominent MOF catalysts under the similar conditions in Table 2. In-pbpta outperforms InPF-110<sup>29</sup> (99%, 3.5 h, solvent-free) and has similar yield as that for  $[[\text{Cd}_2(\text{L})(\text{H}_2\text{O})(\text{DMF})]\cdot 3\text{DMF}\cdot 2\text{H}_2\text{O}]_n$ <sup>82</sup> (98%, 4 h, solvent-free). A higher loading amount (0.88 mol %, Table 3) is needed for In-pbpta compared to that of InPF-110 (0.5 mol %), and at the same loading amount of 0.5 mol %, it shows a lower TON of 168 relative to InPF-110 (198).<sup>29</sup> However, this high yield obtained within such a short

**Table 1. In-pbpta Catalyzed Strecker One-Pot Three Component Reaction with Benzaldehyde and Various Ketones Using Aniline as the Amine<sup>a</sup>**

Entry	Substrate	Product	Conversion <sup>b</sup>	Selectivity <sup>b</sup>	Yield
			(%)	(%)	(%)
1	Benzaldehyde		> 99	> 99	> 99
2	Acetophenone		98	> 99	98
3	Benzophenone		95	> 99	95
4	4-Methylacetophenone		52	> 99	52

<sup>a</sup>Reaction conditions: aldehyde/ketone, aniline, TMS-CN (0.85:0.77:0.85), 10 mg (0.88 mol % based on  $[\text{In}_3\text{O}(\text{pbpta})_{1.5}(\text{H}_2\text{O})_3]$ ) catalyst,  $\text{N}_2$  atmosphere, 25 °C, 30 min; catalyst washed with chloroform. <sup>b</sup>Calculated from <sup>1</sup>H NMR or GC-MS, from reaction crude.

**Table 2. Comparison of the MOF Catalysts for the Strecker Reaction of Acetophenone with Aniline and TMSCN**

MOF catalyst	time	solvent	yield <sup>a</sup> (%)
In-pbpta (this work)	30 min	solvent-free	98
Fe <sub>3</sub> O <sub>4</sub> /MIL-101(Fe) <sup>81</sup>	45 min	EtOH	92
InPF-110 <sup>29</sup>	3.5 h	solvent-free	99
[[Cd <sub>2</sub> (L)(H <sub>2</sub> O)(DMF)]·3DMF·2H <sub>2</sub> O] <sub>n</sub> <sup>82</sup>	4 h	solvent-free	98
[[Zn <sub>2</sub> (3-tpom)(L) <sub>2</sub> ]·2H <sub>2</sub> O] <sub>n</sub> <sup>83</sup>	5 h	solvent-free	90
[[[(CH <sub>3</sub> ) <sub>2</sub> NH <sub>2</sub> ][Zn <sub>2</sub> (L)(H <sub>2</sub> O)PO <sub>4</sub> ]·2DMF] <sub>n</sub> (2') <sup>84</sup>	7 h	solvent-free	89
In <sub>12</sub> -GL <sup>a,33</sup>	24 h	MeOH	99

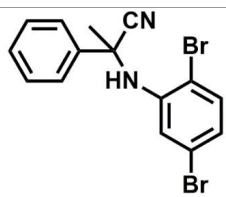
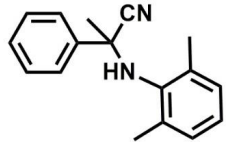
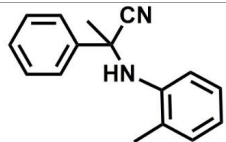
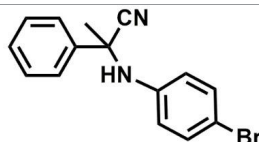
<sup>a</sup>Reaction carried out at 30 °C.

**Table 3. Comparison of the In-pbpta with InPF-110 for the Strecker Reaction of Acetophenone, Aniline, and TMSCN**

MOF catalyst	time	catalyst amount (mol %)	solvent	yield <sup>a</sup> (%)	TON <sup>a</sup>
In-pbpta (this work)	30 min	0.88	solvent-free	98	115
	65 min	0.5		84	168
InPF-110 <sup>29</sup>	3.5 h	0.5	solvent-free	99	198

<sup>a</sup>TON = mmol of substrate/(mmol of catalyst).

**Table 4. In-pbpta Catalyzed Strecker One-Pot Three Component Reaction with Acetophenone as the Ketone and Various Anilines**

Entry	Substrate	Product	Conversion <sup>b</sup>	Selectivity <sup>b</sup>	Yield
			(%)	(%)	(%)
1	2,5-dibromoaniline		98	> 99	98
2	2,6-dimethylaniline		83	> 99	83
3	o-toluidine		75	> 99	75
4	4-bromoaniline		55	> 99	55

<sup>a</sup>Reaction conditions: acetophenone, amine, TMSCN (0.85:0.77:0.85), 10 mg (0.88 mol % based on [In<sub>3</sub>O(pbpta)<sub>1.5</sub>(H<sub>2</sub>O)<sub>3</sub>]) catalyst, N<sub>2</sub> atmosphere, 25 °C, 30 min; catalyst washed with chloroform. <sup>b</sup>Calculated from <sup>1</sup>H NMR or GC-MS, from reaction crude.

time duration of 30 min is one of the highest among the MOF catalysts reported so far. We also performed the blank control reaction with just the benzaldehyde, aniline, and TMSCN and

did not observe the formation of Strecker product, indicating that the catalyst is necessary to get successful conversion. Similarly, reaction of other ketones with aniline and TMSCN

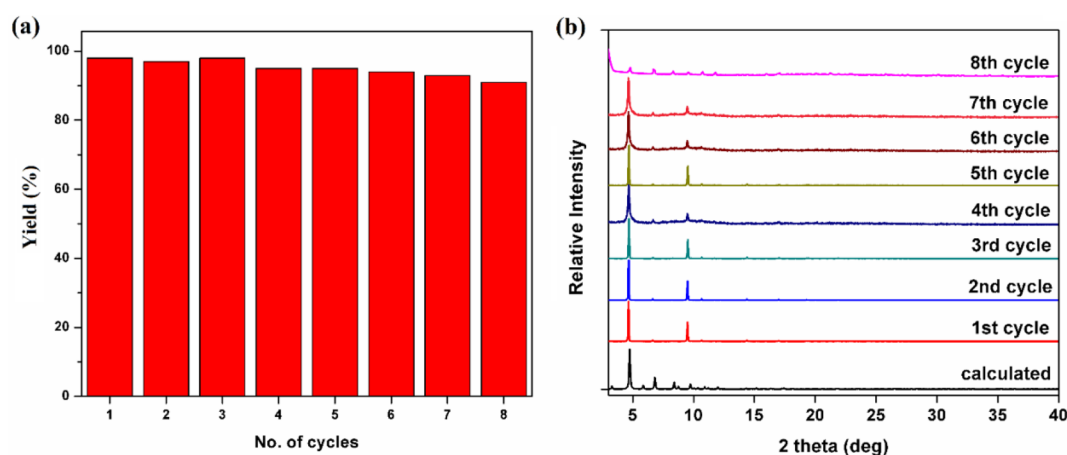


Figure 3. (a) Catalytic activity over eight cycles and (b) PXRD patterns of the MOF after catalytic cycles.

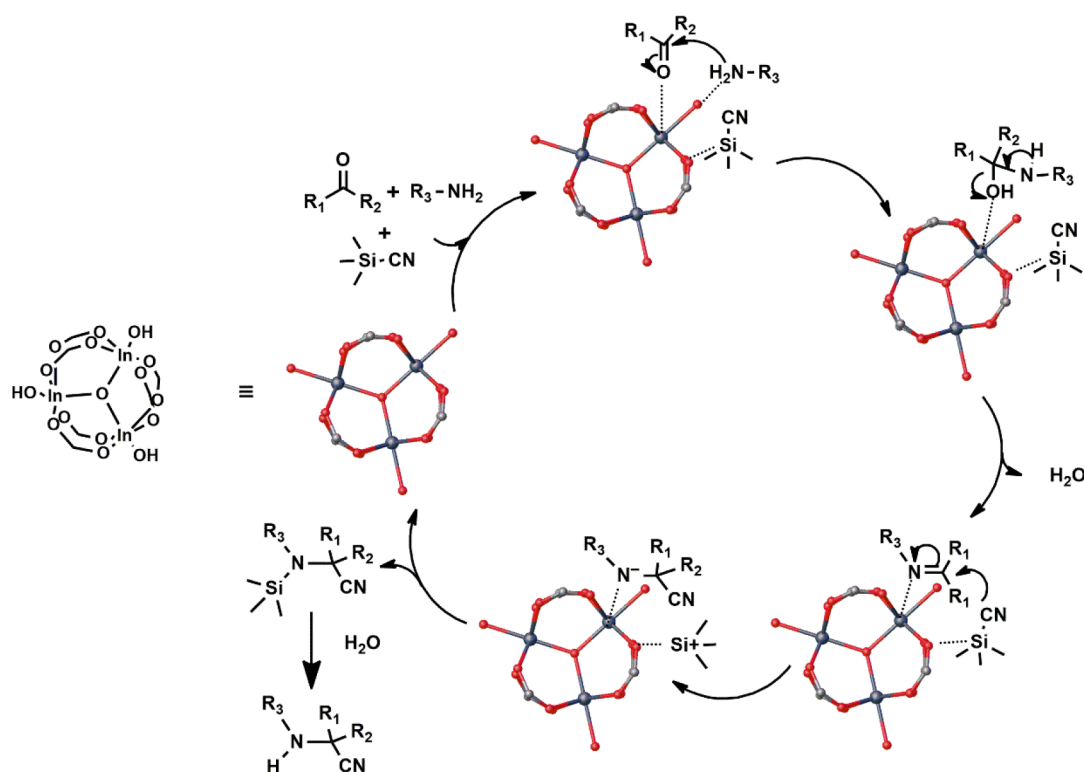


Figure 4. Proposed mechanism of the Strecker reaction between the aldehyde/ketone, amine, and TMSCN.

also proceeded smoothly with good to excellent yield, viz., benzophenone (95%) and 4-methylacetophenone (52%). The yield for 4-methylacetophenone is much less compared to that for InPF-110 (94%, 4 h).

To further explore the scope of other amine counterparts, 2,5-dibromoaniline and 2,6-dimethylaniline were reacted with acetophenone and TMSCN to give excellent yields of 98 and 83%, respectively (Table 4). The electron donating groups with positive inductive effect on carbonyl gave lower yield (Table 1, entry 4), while for the amine components the substituents show a mixed interplay of resonance and inductive effects (Table 4). Finally, the catalyst was subjected to the recyclability tests and could be used for at least five cycles without much significant loss in activity for the Strecker reaction of acetophenone, aniline, and TMSCN (Figure 3a). After the fifth cycle, the yield starts to decrease, indicating a

start of loss in crystallinity, as evident from the PXRD patterns that show a peak broadening after the fourth cycle, and subsequent reduction in the intensity of the peaks after the eighth cycle (Figure 3b). The recovery yield of the catalyst was >99% after each cycle; however, owing to the small amount of the catalyst used, the activated In-pbpta had to be refilled after the fourth cycle. Although the In-pbpta compared to InPF-110<sup>29</sup> showed lesser activity for a broader scope of reagents, still its good performance within a short time duration deems it promising for applicability for the Strecker reaction of specific ketones/anilines and demand further exploration with other aliphatic substrates.

Such high catalytic efficiency of In-pbpta in such a short time duration prompted us to gain a deeper insight into the origin of such high activity and the possible interactions involved. One assumption could be based on the structure,

since In-pbpta features a high density of catalytically active sites and well-defined cavities for the substrate and product diffusion.

According to the mechanism described in earlier reports by Monge et al.<sup>28,29</sup> and others,<sup>27,33,82–85</sup> it has been proposed that the indium metal center acts as the Lewis acid activating the carbonyl and the amine groups and the oxygen of the oxo-bridge acts as a Lewis base interacting with Si of the TMSCN and releasing the cyano ion. In the case of In-pbpta, owing to the presence of pyridyl nitrogen in the ligand and the bridging oxygen in the cluster, both could potentially act as Lewis basic sites. However, in order to achieve the fast formation of the products, the oxygen sites would be preferred. We did carry out theoretical calculations as discussed in the following section on the cluster to establish the presence and activation of substrates around the cluster; however, investigating the whole cluster and ligand subunit would be computationally expensive and was not pursued. After the activation of the carbonyl and amine groups, imine is formed and the imine carbon is then attacked by the CN group from TMSCN which leads to the formation of the  $\alpha$ -aminonitrile (Figure 4). Further studies showed the aniline coordinated to the accessible metal site.<sup>29</sup> However, more investigations were needed for concrete establishment to understand the mechanism of the reaction.

Attempts to crystallize the aniline or aldehyde/ketone were futile as the size of the obtained crystals was very small leading to low resolution on the data; in addition, the substrates would be highly disordered due to the high symmetry of the structure. Kinetic NMR experiments were also carried out, and they showed the very fast formation of imine within 5 min (Figure S6); however, it was difficult to calculate the order and the rate of the reaction in the three components system. We thus resorted to computational studies in an attempt to understand the local environment around the catalytically active indium sites and to find the interactions of the framework with the substrates. Taking inspiration from the previous simulation studies on the MOF-H<sub>2</sub> interactions,<sup>41</sup> this larger system was then targeted.

**3.4. Computational Modeling Analysis.** On the basis of the classical NVT Monte Carlo simulated annealing and then optimizing using plane wave DFT and triple  $\zeta$  basis sets with the CP2K code on a fragment of the MOF; the amino group coordinates one of its H atoms to the nitrate counterions (which are themselves sorbed onto the open metal site). The cyanide sorbate settles into the corners of the MOF formed by the three indium ions and the cyanide functionality oriented parallel to one of the linker rings. The aldehyde sorbate (R = H for simplicity) coordinated with the oxygen facing the cyanide group and the hydrogen toward the nitrate ion (Figure 5).

On the basis of MPMC calculations, the cyanide was dominated by van der Waals, with Coulombic second and induced dipole third. It is sorbed into the corner of the cage primarily due to methyl group interaction with the framework explaining why van der Waals dominates. For the amine, Coulombic dominates (due to the strong interaction with the counterion), followed by induced dipole and the van der Waals. For the aldehyde van der Waals is the strongest, but Coulombic is not far behind (indicating interaction with the counterion and cyanide sorbate, respectively) with induced dipole trailing behind. The cyanide reagent still has van der Waals as the strongest energy component (due to methyl interaction with linker rings), but the electrostatics is over two-thirds as strong and added together with the polarization

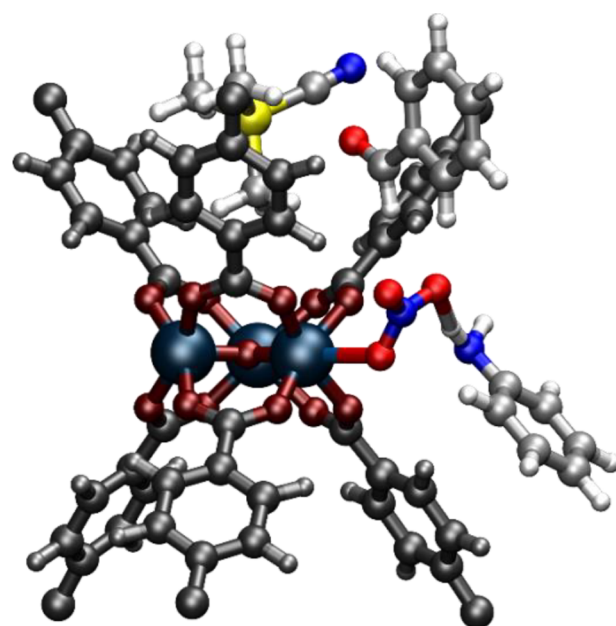


**Figure 5.** Sorption of the aniline, TMSCN, and benzaldehyde about the In-oxo cluster. From NVT calculations.

the total charge component is a bit stronger than the van der Waals.

On the basis of this configuration (Figure 6), we concluded that most likely the nitrate will pull one of the amino

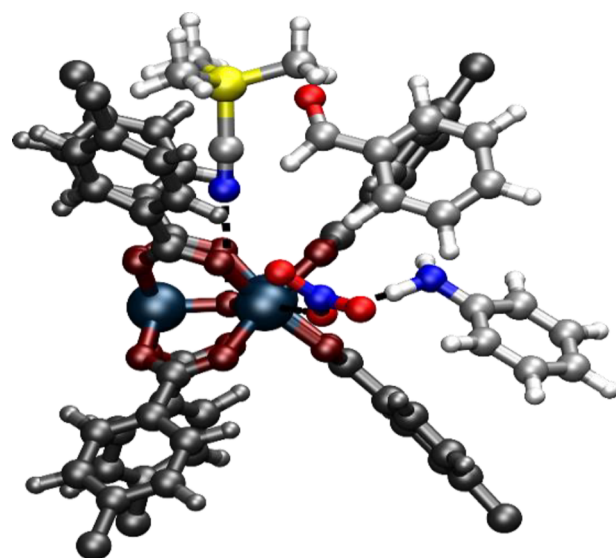


**Figure 6.** MPMC optimized positions and interactions (dotted black lines) of the aniline, TMSCN, and benzaldehyde about the In-oxo cluster.

hydrogens and then the amino nitrogen will coordinate to the indium along with (or replacing entirely) the nitrate. Similar behavior has also been observed in InPF-110, whereby the aniline was observed to coordinate with the indium center having the accessible metal site, and it partly replaced the solvent ligand.<sup>29</sup> The nitrate ion is initially sorbed onto one of the indium atoms, but as it pulls one of the amino hydrogens, the nitrogen will become more attracted to the indium as well as pulling it in toward the cluster. The cyano group also coordinated to the indium, stabilizing it as a cyanide ion.

Thus, the presence of the aldehyde/ketone, amine, and TMSN in close vicinity to each other facilitate the quick formation of the imine followed by immediate attack on the imine to generate the aminonitrile product. Further calculations to study the interaction of imine and TMSCN with the framework will be carried out to gain deeper insights and provide for better design of the catalyst.

#### 4. CONCLUSION

In the present study, we have successfully designed and synthesized a robust In-*soc*-MOF featuring relatively high porosity and accessible open metal sites appropriate for tuning and enhancing interactions with guest molecules. The MOF demonstrated excellent catalysis performance in the Strecker reaction of ketones in a solvent-free environment within 30 min. In addition, the catalyst could be easily recovered and readily recycled. The In-pbpta MOF thus provided a sustainable and efficient catalytic platform for the Strecker synthesis of  $\alpha$ -aminonitriles which can be further hydrolyzed to give the unnatural  $\alpha$ -amino acids. The theoretical calculations suggested an insight about the nature of the interactions involved between the substrates and the In-oxo clusters which can help in further design of the catalysts for better activities. Our work herein thus not only contributes MOF as a new class of efficient heterogeneous catalyst for one-pot Strecker reaction but also paves a way to develop MOF as a new platform for other named reactions in a heterogeneous manner.

#### ■ ASSOCIATED CONTENT

##### SI Supporting Information

The Supporting Information is available free of charge at <https://pubs.acs.org/doi/10.1021/acsami.1c09074>.

Experimental details including TGA, PXRD, NMR spectra, and gas adsorption isotherms (PDF)

#### ■ AUTHOR INFORMATION

##### Corresponding Authors

**Shengqian Ma** – Department of Chemistry, University of North Texas, Denton, Texas 76201, United States; [orcid.org/0000-0002-1897-7069](https://orcid.org/0000-0002-1897-7069); Email: [Shengqian.Ma@unt.edu](mailto:Shengqian.Ma@unt.edu)

**Sanjay Kumar** – Department of Chemistry, Multani Mal Modi College, Patiala 147001 Punjab, India; [orcid.org/0000-0002-6723-5416](https://orcid.org/0000-0002-6723-5416); Email: [sanjay2002@gmail.com](mailto:sanjay2002@gmail.com)

##### Authors

**Gaurav Verma** – Department of Chemistry, University of North Texas, Denton, Texas 76201, United States

**Katherine Forrest** – Department of Chemistry, University of South Florida, Tampa, Florida 33620, United States

**Benjamin A. Carr** – Department of Chemistry & Biochemistry, University of California San Diego, La Jolla, California 92093-0021, United States

**Harsh Vardhan** – Department of Chemistry, University of South Florida, Tampa, Florida 33620, United States

**Junyu Ren** – Department of Chemistry, University of North Texas, Denton, Texas 76201, United States

**Tony Pham** – Department of Chemistry, University of South Florida, Tampa, Florida 33620, United States; [orcid.org/0000-0001-5654-163X](https://orcid.org/0000-0001-5654-163X)

**Brian Space** – Department of Chemistry, University of South Florida, Tampa, Florida 33620, United States; Department of Chemistry, North Carolina State University, Raleigh, North Carolina 27607, United States

Complete contact information is available at: <https://pubs.acs.org/doi/10.1021/acsami.1c09074>

#### Notes

The authors declare no competing financial interest.

#### ■ ACKNOWLEDGMENTS

We acknowledge the Robert A. Welch Foundation (B-0027) for financial support of this work. We thank the USF X-ray Diffraction Facility and Solid-State Characterization Core Lab for the single crystal and powder X-ray diffraction measurements, the Chemical Purification Analysis and Screening Core Facility (CPAS) at USF for the GC-MS measurements, and the USF Interdisciplinary NMR Facility (USF NMRF) for the NMR data.

#### ■ REFERENCES

- (1) Myers, S. S.; Gaffikin, L.; Golden, C. D.; Ostfeld, R. S.; Redford, K. H.; Ricketts, T. H.; Turner, W. R.; Osofsky, S. A. Human Health Impacts of Ecosystem Alteration. *Proc. Natl. Acad. Sci. U. S. A.* **2013**, *110*, 18753–18760.
- (2) Martin, J.-L.; Maris, V.; Simberloff, D. S. The Need to Respect Nature and its Limits Challenges Society and Conservation Science. *Proc. Natl. Acad. Sci. U. S. A.* **2016**, *113*, 6105–6112.
- (3) *The Sustainable Development Goals Report 2019*; United Nations, 2019.
- (4) Hayashi, Y. Pot Economy and One-Pot Synthesis. *Chem. Sci.* **2016**, *7*, 866–880.
- (5) Zhao, W.; Chen, F.-E. One-Pot Synthesis and Its Practical Application in Pharmaceutical Industry. *Curr. Org. Synth.* **2012**, *9*, 873–897.
- (6) Varma, R. S. Greener and Sustainable Trends in Synthesis of Organics and Nanomaterials. *ACS Sustainable Chem. Eng.* **2016**, *4*, 5866–5878.
- (7) Kouznetsov, V. V.; Galvis, C. E. P. Strecker Reaction and  $\alpha$ -amino nitriles: Recent Advances in their Chemistry, Synthesis, and Biological Properties. *Tetrahedron* **2018**, *74*, 773–810.
- (8) José Climent, M.; Corma, A.; Iborra, S. Homogeneous and Heterogeneous Catalysts for Multicomponent Reactions. *RSC Adv.* **2012**, *2*, 16–58.
- (9) Merino, P.; Marqués-López, E.; Tejero, T.; Herrera, R. P. Organocatalyzed Strecker Reactions. *Tetrahedron* **2009**, *65*, 1219–1234.
- (10) Radai, Z.; Kiss, N. Z.; Keglevich, G. An Overview of the Applications of Ionic Liquids as Catalysts and Additives in Organic Chemical Reactions. *Curr. Org. Chem.* **2018**, *22*, 533–556.
- (11) Marqués-López, E.; Herrera, R. P. Bucherer-Bergs and Strecker Multicomponent Reactions. *In Multicomponent Reactions* **2015**, 331–357.
- (12) Pimparkar, S.; Koodan, A.; Maiti, S.; Ahmed, N. S.; Mostafa, M. M.; Maiti, D. C-CN Bond Formation: An Overview of Diverse Strategies. *Chem. Commun.* **2021**, *57*, 2210–2232.
- (13) Bavykina, A.; Kolobov, N.; Khan, I. S.; Bau, J. A.; Ramirez, A.; Gascon, J. Metal-Organic Frameworks in Heterogeneous Catalysis: Recent Progress, New Trends, and Future Perspectives. *Chem. Rev.* **2020**, *120*, 8468–8535.
- (14) Jiao, L.; Wang, Y.; Jiang, H.-L.; Xu, Q. Metal-Organic Frameworks as Platforms for Catalytic Applications. *Adv. Mater.* **2018**, *30*, 1703663.
- (15) Kang, Y.-S.; Lu, Y.; Chen, K.; Zhao, Y.; Wang, P.; Sun, W.-Y. Metal-Organic Frameworks with Catalytic Centers: From Synthesis to Catalytic Application. *Coord. Chem. Rev.* **2019**, *378*, 262–280.



- (16) Zhou, H.-C.; Long, J. R.; Yaghi, O. M. Introduction to Metal-Organic Frameworks. *Chem. Rev.* **2012**, *112* (2), 673–674.
- (17) Hendon, C. H.; Rieth, A. J.; Korzyński, M. D.; Dincă, M. Grand Challenges and Future Opportunities for Metal-Organic Frameworks. *ACS Cent. Sci.* **2017**, *3*, 554–563.
- (18) Pascanu, V.; González Miera, G.; Inge, A. K.; Martín-Matute, B. Metal-Organic Frameworks as Catalysts for Organic Synthesis: A Critical Perspective. *J. Am. Chem. Soc.* **2019**, *141*, 7223–7234.
- (19) Dhakshinamoorthy, A.; Alvaro, M.; Garcia, H. Metal-organic Frameworks As Heterogeneous Catalysts for Oxidation Reactions. *Catal. Sci. Technol.* **2011**, *1*, 856–867.
- (20) Dhakshinamoorthy, A.; Opanasenko, M.; Čejka, J.; Garcia, H. Metal Organic Frameworks as Heterogeneous Catalysts for the Production of Fine Chemicals. *Catal. Sci. Technol.* **2013**, *3*, 2509–2540.
- (21) Gascon, J.; Corma, A.; Kapteijn, F.; Llabrés i Xamena, F. X. Metal Organic Framework Catalysis: Quo vadis? *ACS Catal.* **2014**, *4*, 361–378.
- (22) Dhakshinamoorthy, A.; Garcia, H. Cascade Reactions Catalyzed by Metal Organic Frameworks. *ChemSusChem* **2014**, *7*, 2392–2410.
- (23) Huang, Y.-B.; Liang, J.; Wang, X.-S.; Cao, R. Multifunctional Metal-Organic Framework Catalysts: Synergistic Catalysis and Tandem Reactions. *Chem. Soc. Rev.* **2017**, *46*, 126–157.
- (24) Aguirre-Díaz, L. M.; Iglesias, M.; Snejko, N.; Gutiérrez-Puebla, E.; Monge, M. A. Indium Metal-Organic Frameworks as Catalysts in Solvent-Free Cyanosilylation Reaction. *CrystEngComm* **2013**, *15*, 9562–9571.
- (25) Martin, O.; Martín, A. J.; Mondelli, C.; Mitchell, S.; Segawa, T. F.; Hauert, R.; Drouilly, C.; Curulla-Ferré, D.; Pérez-Ramírez, J. Indium Oxide as a Superior Catalyst for Methanol Synthesis by CO<sub>2</sub> Hydrogenation. *Angew. Chem., Int. Ed.* **2016**, *55*, 6261–6265.
- (26) Brandão, P.; Burke, A. J.; Pineiro, M. A Decade of Indium-Catalyzed Multicomponent Reactions (MCRs). *Eur. J. Org. Chem.* **2020**, *2020*, 5501–5513.
- (27) Xia, J.; Xu, J. N.; Fan, Y.; Song, T. Y.; Wang, L.; Zheng, J. F. Indium Metal-Organic Frameworks as High-Performance Heterogeneous Catalysts for the Synthesis of Amino Acid Derivatives. *Inorg. Chem.* **2014**, *53*, 10024–10026.
- (28) Aguirre-Díaz, L. M.; Gandara, F.; Iglesias, M.; Snejko, N.; Gutierrez-Puebla, E.; Monge, M. A. Tunable Catalytic Activity of Solid Solution Metal-Organic Frameworks in One-Pot Multi-component Reactions. *J. Am. Chem. Soc.* **2015**, *137*, 6132–6135.
- (29) Reinares-Fisac, D.; Aguirre-Díaz, L. M.; Iglesias, M.; Snejko, N.; Gutierrez-Puebla, E.; Monge, M. A.; Gandara, F. A Mesoporous Indium Metal-Organic Framework: Remarkable Advances in Catalytic Activity for Strecker Reaction of Ketones. *J. Am. Chem. Soc.* **2016**, *138*, 9089–9092.
- (30) Chai, J.; Wang, P. C.; Jia, J.; Ma, B.; Sun, J.; Tao, Y. F.; Zhang, P.; Wang, L.; Fan, Y. In(III) and Sc(III) Based Coordination Polymers Derived from Rigid Benzimidazole-5,6-dicarboxylic acid: Synthesis, Crystal Structure and Catalytic Property. *Polyhedron* **2018**, *141*, 369–376.
- (31) Chai, J.; Zhang, P.; Xu, J. N.; Qi, H.; Sun, J.; Jing, S. B.; Chen, X. D.; Fan, Y.; Wang, L. An In-based 3D Metal-Organic Framework as Heterogeneous Lewis Acid Catalyst for Multi-Component Strecker Reactions. *Inorg. Chim. Acta* **2018**, *479*, 165–171.
- (32) Chen, H. T.; Fan, L. M.; Zhang, X. T.; Ma, L. F. Nanocage-Based In(III){Tb-III}(2)-Organic Framework Featuring Lotus-Shaped Channels for Highly Efficient CO<sub>2</sub> Fixation and I<sub>2</sub> Capture. *ACS Appl. Mater. Interfaces* **2020**, *12*, 27803–27811.
- (33) Liang, G. M.; Xiong, P.; Azam, K.; Ni, Q. L.; Zeng, J. Q.; Gui, L. C.; Wang, X. J. A Discrete Tetrahedral Indium Cage as an Efficient Heterogeneous Catalyst for the Fixation of CO<sub>2</sub> and the Strecker Reaction of Ketones. *Inorg. Chem.* **2020**, *59*, 1653–1659.
- (34) Yuan, Y.; Li, J.; Sun, X.; Li, G.; Liu, Y.; Verma, G.; Ma, S. Indium-Organic Frameworks Based on Dual Secondary Building Units Featuring Halogen-Decorated Channels for Highly Effective CO<sub>2</sub> Fixation. *Chem. Mater.* **2019**, *31*, 1084–1091.
- (35) Verma, G.; Kumar, S.; Vardhan, H.; Ren, J.; Niu, Z.; Pham, T.; Wojtas, L.; Butikofer, S.; Echeverria Garcia, J. C.; Chen, Y.-S.; Space, B.; Ma, S. A Robust soc-MOF Platform Exhibiting High Gravimetric Uptake and Volumetric Deliverable Capacity for On-Board Methane Storage. *Nano Res.* **2021**, *14*, 512–517.
- (36) Liu, Y.; Eubank, J. F.; Cairns, A. J.; Eckert, J.; Kravtsov, V. C.; Luebke, R.; Eddaoudi, M. Assembly of Metal-Organic Frameworks (MOFs) Based on Indium-Trimer Building Blocks: A Porous MOF with soc Topology and High Hydrogen Storage. *Angew. Chem., Int. Ed.* **2007**, *46*, 3278–3283.
- (37) Alezi, D.; Belmabkhout, Y.; Suyetin, M.; Bhatt, P. M.; Weseliński, L. J.; Solovyeva, V.; Adil, K.; Spanopoulos, I.; Trikalitis, P. N.; Emwas, A.-H.; Eddaoudi, M. MOF Crystal Chemistry Paving the Way to Gas Storage Needs: Aluminum-Based soc-MOF for CH<sub>4</sub>, O<sub>2</sub>, and CO<sub>2</sub> Storage. *J. Am. Chem. Soc.* **2015**, *137*, 13308–13318.
- (38) Towsif Abtab, S. M.; Alezi, D.; Bhatt, P. M.; Shkurenko, A.; Belmabkhout, Y.; Aggarwal, H.; Weseliński, L. J.; Alsadun, N.; Samin, U.; Hedhili, M. N.; Eddaoudi, M. Reticular Chemistry in Action: A Hydrolytically Stable MOF Capturing Twice Its Weight in Adsorbed Water. *Chem.* **2018**, *4*, 94–105.
- (39) Moellmer, J.; Celer, E. B.; Luebke, R.; Cairns, A. J.; Staudt, R.; Eddaoudi, M.; Thommes, M. Insights on Adsorption Characterization of Metal-Organic Frameworks: A Benchmark Study on the Novel soc-MOF. *Microporous Mesoporous Mater.* **2010**, *129*, 345–353.
- (40) Pang, M. L.; Cairns, A. J.; Liu, Y. L.; Belmabkhout, Y.; Zeng, H. C.; Eddaoudi, M. Highly Monodisperse M-III-Based soc-MOFs (M = In and Ga) with Cubic and Truncated Cubic Morphologies. *J. Am. Chem. Soc.* **2012**, *134*, 13176–13179.
- (41) Pham, T.; Forrest, K. A.; Hogan, A.; Tudor, B.; McLaughlin, K.; Belof, J. L.; Eckert, J.; Space, B. Understanding Hydrogen Sorption in In-soc-MOF: A Charged Metal-Organic Framework with Open-Metal Sites, Narrow Channels, and Counterions. *Cryst. Growth Des.* **2015**, *15*, 1460–1471.
- (42) Cairns, A. J.; Eckert, J.; Wojtas, L.; Thommes, M.; Wallacher, D.; Georgiev, P. A.; Forster, P. M.; Belmabkhout, Y.; Ollivier, J.; Eddaoudi, M. Gaining Insights on the H<sub>2</sub>-Sorbent Interactions: Robust soc-MOF Platform as a Case Study. *Chem. Mater.* **2016**, *28*, 7353–7361.
- (43) Zheng, B.; Sun, X. D.; Li, G. H.; Cairns, A. J.; Kravtsov, V. C.; Huo, Q. S.; Liu, Y. L.; Eddaoudi, M. Solvent-Controlled Assembly of Ionic Metal-Organic Frameworks Based on Indium and Tetracarboxylate Ligand: Topology Variety and Gas Sorption Properties. *Cryst. Growth Des.* **2016**, *16*, 5554–5562.
- (44) Wang, B.; Yang, Q.; Guo, C.; Sun, Y. X.; Xie, L. H.; Li, J. R. Stable Zr(IV)-Based Metal-Organic Frameworks with Predesigned Functionalized Ligands for Highly Selective Detection of Fe(III) Ions in Water. *ACS Appl. Mater. Interfaces* **2017**, *9*, 10286–10295.
- (45) Bratsos, I.; Tampaxis, C.; Spanopoulos, I.; Demitri, N.; Charalambopoulou, G.; Vourloumis, D.; Steriotis, T. A.; Trikalitis, P. N. Heterometallic In(III)-Pd(II) Porous Metal-Organic Framework with Square-Octahedron Topology Displaying High CO<sub>2</sub> Uptake and Selectivity toward CH<sub>4</sub> and N<sub>2</sub>. *Inorg. Chem.* **2018**, *57*, 7244–7251.
- (46) Kapustin, E. A. A Crystal with Nearly 200% of Its Body Weight in Water. *Chem.* **2018**, *4*, 16–17.
- (47) Liu, H. Y.; Gao, G. M.; Bao, F. L.; Wei, Y. H.; Wang, H. Y. Enhanced Water Stability and Selective Carbon Dioxide Adsorption of a soc-MOF with Amide-Functionalized Linkers. *Polyhedron* **2019**, *160*, 207–212.
- (48) Feng, Y.; Wang, Z. K.; Fan, W. D.; Kang, Z. X.; Feng, S.; Fan, L. L.; Hu, S. Q.; Sun, D. F. Engineering the Pore Environment of Metal-Organic Framework Membranes via Modification of the Secondary Building Unit for Improved Gas Separation. *J. Mater. Chem. A* **2020**, *8*, 13132–13141.
- (49) Cuadrado-Collados, C.; Mouchaham, G.; Daemen, L.; Cheng, Y. Q.; Ramirez-Cuesta, A.; Aggarwal, H.; Missyul, A.; Eddaoudi, M.; Belmabkhout, Y.; Silvestre-Albero, J. Quest for an Optimal Methane Hydrate Formation in the Pores of Hydrolytically Stable Metal-Organic Frameworks. *J. Am. Chem. Soc.* **2020**, *142*, 13391–13397.

- (50) Kalmutzki, M. J.; Hanikel, N.; Yaghi, O. M. Secondary Building Units as the Turning Point in the Development of the Reticular Chemistry of MOFs. *Sci. Adv.* **2018**, *4*, eaat9180.
- (51) Verma, G.; Kumar, S.; Pham, T.; Niu, Z.; Wojtas, L.; Perman, J. A.; Chen, Y.-S.; Ma, S. Partially Interpenetrated NbO Topology Metal-Organic Framework Exhibiting Selective Gas Adsorption. *Cryst. Growth Des.* **2017**, *17*, 2711–2717.
- (52) Anderson, J. A.; Jankowski, E.; Grubb, T. L.; Engel, M.; Glotzer, S. C. Massively Parallel Monte Carlo for Many-Particle Simulations on GPUs. *J. Comput. Phys.* **2013**, *254*, 27–38.
- (53) Jorgensen, W. L.; Maxwell, D. S.; Tirado-Rives, J. Development and Testing of the OPLS All-Atom Force Field on Conformational Energetics and Properties of Organic Liquids. *J. Am. Chem. Soc.* **1996**, *118*, 11225–11236.
- (54) Sambasivarao, S. V.; Acevedo, O. Development of OPLS-AA Force Field Parameters for 68 Unique Ionic Liquids. *J. Chem. Theory Comput.* **2009**, *5*, 1038–1050.
- (55) Rappe, A. K.; Casewit, C. J.; Colwell, K. S.; Goddard, W. A.; Skiff, W. M. UFF, A Full Periodic Table Force Field for Molecular Mechanics and Molecular Dynamics Simulations. *J. Am. Chem. Soc.* **1992**, *114*, 10024–10035.
- (56) Wilmer, C. E.; Kim, K. C.; Snurr, R. Q. An Extended Charge Equilibration Method. *J. Phys. Chem. Lett.* **2012**, *3*, 2506–2511.
- (57) Belof, J. L.; Stern, A. C.; Eddaoudi, M.; Space, B. On the Mechanism of Hydrogen Storage in a Metal-Organic Framework Material. *J. Am. Chem. Soc.* **2007**, *129*, 15202–15210.
- (58) Aprà, E.; Bylaska, E. J.; de Jong, W. A.; Govind, N.; Kowalski, K.; Straatsma, T. P.; Valiev, M.; van Dam, H. J. J.; Alexeev, Y.; Anchell, J.; Anisimov, V.; Aquino, F. W.; Atta-Fynn, R.; Autschbach, J.; Bauman, N. P.; Becca, J. C.; Bernholdt, D. E.; Bhaskaran-Nair, K.; Bogatko, S.; Borowski, P.; Boschen, J.; Brabec, J.; Bruner, A.; Cauët, E.; Chen, Y.; Chuev, G. N.; Cramer, C. J.; Daily, J.; Deegan, M. J. O.; Dunning, T. H.; Dupuis, M.; Dylla, K. G.; Fann, G. I.; Fischer, S. A.; Fonari, A.; Früchtl, H.; Gagliardi, L.; Garza, J.; Gawande, N.; Ghosh, S.; Glaesemann, K.; Götz, A. W.; Hammond, J.; Helms, V.; Hermes, E. D.; Hirao, K.; Hirata, S.; Jacquelin, M.; Jensen, L.; Johnson, B. G.; Jónsson, H.; Kendall, R. A.; Klemm, M.; Kobayashi, R.; Konkov, V.; Krishnamoorthy, S.; Krishnan, M.; Lin, Z.; Lins, R. D.; Littlefield, R. J.; Logsdail, A. J.; Lopata, K.; Ma, W.; Marenich, A. V.; Martin del Campo, J.; Mejia-Rodriguez, D.; Moore, J. E.; Mullin, J. M.; Nakajima, T.; Nascimento, D. R.; Nichols, J. A.; Nichols, P. J.; Nieplocha, J.; Otero-de-la-Roza, A.; Palmer, B.; Panyala, A.; Pirojsirikul, T.; Peng, B.; Peverati, R.; Pittner, J.; Pollack, L.; Richard, R. M.; Sadayappan, P.; Schatz, G. C.; Shelton, W. A.; Silverstein, D. W.; Smith, D. M. A.; Soares, T. A.; Song, D.; Swart, M.; Taylor, H. L.; Thomas, G. S.; Tipparaju, V.; Truhlar, D. G.; Tsemekhman, K.; Van Voorhis, T.; Vázquez-Mayagoitia, Á.; Verma, P.; Villa, O.; Vishnu, A.; Vogiatzis, K. D.; Wang, D.; Weare, J. H.; Williamson, M. J.; Windus, T. L.; Woliński, K.; Wong, A. T.; Wu, Q.; Yang, C.; Yu, Q.; Zacharias, M.; Zhang, Z.; Zhao, Y.; Harrison, R. J. NWChem: Past, Present, and Future. *J. Chem. Phys.* **2020**, *152*, 184102.
- (59) Kühne, T. D.; Iannuzzi, M.; Del Ben, M.; Rybkin, V. V.; Seewald, P.; Stein, F.; Laino, T.; Khaliullin, R. Z.; Schütt, O.; Schiffmann, F.; Golze, D.; Wilhelm, J.; Chulkov, S.; Bani-Hashemian, M. H.; Weber, V.; Borštnik, U.; Taillefumier, M.; Jakobovits, A. S.; Lazzaro, A.; Pabst, H.; Müller, T.; Schade, R.; Guidon, M.; Andermatt, S.; Holmberg, N.; Schenter, G. K.; Hehn, A.; Bussy, A.; Belleflamme, F.; Tabacchi, G.; GlöB, A.; Lass, M.; Bethune, I.; Mundy, C. J.; Plessl, C.; Watkins, M.; VandeVondele, J.; Krack, M.; Hutter, J. CP2K: An Electronic Structure and Molecular Dynamics Software Package - Quickstep: Efficient and Accurate Electronic Structure Calculations. *J. Chem. Phys.* **2020**, *152*, 194103.
- (60) Lehtola, S.; Steigemann, C.; Oliveira, M. J. T.; Marques, M. A. L. Recent Developments in Libxc -A Comprehensive Library of Functionals for Density Functional Theory. *SoftwareX* **2018**, *7*, 1–5.
- (61) Schütt, O.; Messmer, P.; Hutter, J.; VandeVondele, J. GPU-Accelerated Sparse Matrix-Matrix Multiplication for Linear Scaling Density Functional Theory. In *Electronic Structure Calculations on Graphics Processing Units* **2016**, 173–190.
- (62) Borštnik, U.; VandeVondele, J.; Weber, V.; Hutter, J. Sparse Matrix Multiplication: The Distributed Block-Compressed Sparse Row Library. *Parallel Comput.* **2014**, *40*, 47–58.
- (63) Hutter, J.; Iannuzzi, M.; Schiffmann, F.; VandeVondele, J. CP2K: Atomistic Simulations of Condensed Matter Systems. *Wires Comput. Mol. Sci.* **2014**, *4*, 15–25.
- (64) Marek, A.; Blum, V.; Johanni, R.; Havu, V.; Lang, B.; Auckenthaler, T.; Heinecke, A.; Bungartz, H. J.; Lederer, H. The ELPA Library: Scalable Parallel Eigenvalue Solutions for Electronic Structure Theory and Computational Science. *J. Phys.: Condens. Matter* **2014**, *26*, 213201.
- (65) Sabatini, R.; Gorni, T.; de Gironcoli, S. Nonlocal van der Waals Density Functional made Simple and Efficient. *Phys. Rev. B: Condens. Matter Mater. Phys.* **2013**, *87*, 041108.
- (66) Marques, M. A. L.; Oliveira, M. J. T.; Burnus, T. Libxc: A library of Exchange and Correlation Functionals for Density Functional Theory. *Comput. Phys. Commun.* **2012**, *183*, 2272–2281.
- (67) Román-Pérez, G.; Soler, J. M. Efficient Implementation of a van der Waals Density Functional: Application to Double-Wall Carbon Nanotubes. *Phys. Rev. Lett.* **2009**, *103*, 096102.
- (68) VandeVondele, J.; Hutter, J. Gaussian Basis Sets for Accurate Calculations on Molecular Systems in Gas and Condensed Phases. *J. Chem. Phys.* **2007**, *127*, 114105.
- (69) Kühne, T. D.; Krack, M.; Mohamed, F. R.; Parrinello, M. Efficient and Accurate Car-Parrinello-like Approach to Born-Oppenheimer Molecular Dynamics. *Phys. Rev. Lett.* **2007**, *98*, 066401.
- (70) Krack, M. Pseudopotentials for H to Kr Optimized for Gradient-Corrected Exchange-Correlation Functionals. *Theor. Chem. Acc.* **2005**, *114*, 145–152.
- (71) VandeVondele, J.; Krack, M.; Mohamed, F.; Parrinello, M.; Chassaing, T.; Hutter, J. Quickstep: Fast and Accurate Density Functional Calculations Using a Mixed Gaussian and Plane Waves Approach. *Comput. Phys. Commun.* **2005**, *167*, 103–128.
- (72) Frigo, M.; Johnson, S. G. The Design and Implementation of FFTW3. *Proc. IEEE* **2005**, *93*, 216–231.
- (73) Kolafa, J. Time-Reversible Always Stable Predictor-Corrector Method for Molecular Dynamics of Polarizable Molecules. *J. Comput. Chem.* **2004**, *25*, 335–342.
- (74) VandeVondele, J.; Hutter, J. An Efficient Orbital Transformation Method for Electronic Structure Calculations. *J. Chem. Phys.* **2003**, *118*, 4365–4369.
- (75) Hartwigsen, C.; Goedecker, S.; Hutter, J. Relativistic Separable Dual-Space Gaussian Pseudopotentials from H to Rn. *Phys. Rev. B: Condens. Matter Mater. Phys.* **1998**, *58*, 3641–3662.
- (76) Lippert, G.; Hutter, J.; Parrinello, M. A Hybrid Gaussian and Plane Wave Density Functional Scheme. *Mol. Phys.* **1997**, *92*, 477–488.
- (77) Goedecker, S.; Teter, M.; Hutter, J. Separable Dual-Space Gaussian Pseudopotentials. *Phys. Rev. B: Condens. Matter Mater. Phys.* **1996**, *54*, 1703–1710.
- (78) Byrd, R. H.; Lu, P.; Nocedal, J.; Zhu, C. A Limited Memory Algorithm for Bound Constrained Optimization. *SIAM J. Sci. Comput.* **1995**, *16*, 1190–1208.
- (79) Spek, A. Structure Validation in Chemical Crystallography. *Acta Crystallogr., Sect. D: Biol. Crystallogr.* **2009**, *65*, 148–155.
- (80) Zhai, Q.-G.; Bu, X.; Mao, C.; Zhao, X.; Feng, P. Systematic and Dramatic Tuning on Gas Sorption Performance in Heterometallic Metal-Organic Frameworks. *J. Am. Chem. Soc.* **2016**, *138*, 2524–2527.
- (81) Mostafavi, M. M.; Movahedi, F. Fe<sub>3</sub>O<sub>4</sub>/MIL-101(Fe) Nanocomposite as an Efficient and Recyclable Catalyst for Strecker Reaction. *Appl. Organomet. Chem.* **2018**, *32*, No. e4217.
- (82) Verma, A.; Tomar, K.; Bharadwaj, P. K. Chiral Cadmium(II) Metal-Organic Framework from an Achiral Ligand by Spontaneous Resolution: An Efficient Heterogeneous Catalyst for the Strecker Reaction of Ketones. *Inorg. Chem.* **2017**, *56*, 13629–13633.
- (83) Gupta, V.; Mandal, S. K. A Microporous Metal-Organic Framework Catalyst for Solvent-free Strecker Reaction and CO<sub>2</sub> Fixation at Ambient Conditions. *Inorg. Chem.* **2020**, *59*, 4273–4281.

(84) Gupta, M.; De, D.; Tomar, K.; Bharadwaj, P. K. From Zn(II)-Carboxylate to Double-Walled Zn(II)-Carboxylato Phosphate MOF: Change in the Framework Topology, Capture and Conversion of CO<sub>2</sub>, and Catalysis of Strecker Reaction. *Inorg. Chem.* **2017**, *56*, 14605–14611.

(85) Gupta, V.; Mandal, S. K. Design and Construction of a Chiral Cd(II)-MOF from Achiral Precursors: Synthesis, Crystal Structure and Catalytic Activity toward C-C and C-N Bond Forming Reactions. *Inorg. Chem.* **2019**, *58*, 3219–3226.

(86) Note: While we were working on In-pbpta, we noticed the report of another MOF FJU-10 with a structure similar to that of In-pbpta, which was synthesized under different reaction conditions and had a slightly different unit cell: Liu, L.; Yao, Z.; Ye, Y.; Liu, C.; Lin, Q.; Chen, S.; Xiang, S.; Zhang, Z. Enhancement of Intrinsic Proton Conductivity and Aniline Sensitivity by Introducing Dye Molecules into the MOF Channel. *ACS Appl. Mater. Interfaces* **2019**, *11*, 16490–16495.